

Imaging Dendritic Spines in *Caenorhabditis elegans*

Andrea Cuentas-Condori¹, D. M. Miller III^{1,2}

¹ Department of Cell and Developmental Biology, Vanderbilt University ² Program of Neuroscience, Vanderbilt University

Corresponding Author

D. M. Miller
david.miller@vanderbilt.edu

Citation

Cuentas-Condori, A., Miller III, D.M. Imaging Dendritic Spines in *Caenorhabditis elegans*. *J. Vis. Exp.* (175), e62676, doi:10.3791/62676 (2021).

Date Published

September 27, 2021

DOI

10.3791/62676

URL

jove.com/video/62676

Abstract

Dendritic spines are specialized sites of synaptic innervation modulated by activity and serve as substrates for learning and memory. Recently, dendritic spines have been described for DD GABAergic neurons as the input sites from presynaptic cholinergic neurons in the motor circuit of *Caenorhabditis elegans*. This synaptic circuit can now serve as a powerful new *in vivo* model of spine morphogenesis and function that exploits the facile genetics and ready accessibility of *C. elegans* to live-cell imaging.

This protocol describes experimental strategies for assessing DD spine structure and function. In this approach, a super-resolution imaging strategy is used to visualize the intricate shapes of actin-rich dendritic spines. To evaluate the DD spine function, the light-activated opsin, Chrimson, stimulates the presynaptic cholinergic neurons, and the calcium indicator, GCaMP, reports the evoked calcium transients in postsynaptic DD spines. Together, these methods comprise powerful approaches for identifying genetic determinants of dendritic spines in *C. elegans* that could also direct spine morphogenesis and function in the brain.

Introduction

Dendritic spines are specialized cellular structures that receive input from neighboring neurons for synaptic transmission. Activation of neurotransmitter receptors elevates intracellular calcium and downstream signaling pathways in these characteristic neuronal protrusions¹. Because of the fundamental importance of dendritic spines to neurotransmission and their misregulation in neurodevelopmental diseases¹, the discovery of factors that

modulate dendritic spine morphogenesis and function is of high interest to the field of neuroscience.

Recently, dendritic spines have been identified in the *C. elegans* nervous system based on key characteristics shared with mammalian spines². This determination is crucial because it opens the possibility of exploiting the advantages of *C. elegans* to investigate spine biology. Dendritic spines on Dorsal D (DD) motor neurons receive input from cholinergic neurons (VA and VB) in the ventral nerve cord (**Figure 1A**)^{2,3,4}. Here, imaging methods are presented to explore

the structure of DD dendritic spines and their function *in vivo* in an intact nervous system that is readily accessible to live imaging and genetic analysis. For monitoring the shape of dendritic spines, (1) cytosolic fluorescent proteins, which fill the dendritic process and spines; (2) membrane-bound fluorescent proteins, which decorate the border of dendritic spines and dendrites; or (3) the actin markers, LifeAct⁵ or Utrophin⁶, which are enriched in dendritic spines are used, thus revealing their shape. To monitor the functionality of DD spines, GCaMP fluorescence is used to detect Ca⁺⁺ transients evoked by activation of the red-shifted opsin, Chrimson, in presynaptic cholinergic neurons⁷. Both strategies are expected to facilitate the study of DD dendritic spines in wild-type and mutant animals.

Protocol

1. Determination of the structure of the DD dendritic spines

1. Create transgenic worms to label DD spines
 1. Use the *flp-13* promoter to build an expression vector for the label of interest (e.g., cytoplasmic mCherry, MYR::mRuby, LifeAct::GFP, GFP::utrophin) (**Figure 1**). See the complete list of plasmids in **Supplementary File 1**.
 2. Use established methods to generate a transgenic line labeling DD spines^{8,9}.
2. Prepare the sealant
 1. Make a 1:1 mixture of paraffin-based embedding medium¹⁰ (see **Table of Materials**).
 2. Heat the medium at 60 °C until melting, then aliquot in 1.5 mL capped microcentrifuge tubes and maintain a heating block at 60-70 °C.

NOTE: Sealant can last for 4 weeks in the heating block.

3. Prepare an anesthetic.
 1. Make stock solutions in distilled H₂O of 1% Tricaine and 1 M levamisole (see **Table of Materials**). Store at -20 °C.
 2. Prepare a working solution of 0.05% Tricaine and 15 mM levamisole anesthetic, as described in steps 1.3.3-1.3.5¹¹.
 3. Mix 75 µL of 1% Tricaine stock and 22.5 µL of 1 M levamisole.
 4. Add M9 buffer to a final volume of 1.5 mL.
 5. Aliquot 10 µL of 0.05% Tricaine, 15 mM levamisole into 0.5 mL microcentrifuge tubes and store at -20 °C.

NOTE: The anesthetic mixture is sensitive to temperature, and individual aliquots of the working solution should not be refrozen after thawing for each experiment. See **Supplementary File 2** for a recipe for M9 buffer.
4. Acquire high-resolution images
 1. Prepare 10% agarose and maintain it in the water bath at 60 °C.

NOTE: See the report by Monica Driscoll in WormBook¹².
 2. Mount 15-20 young adults on 10% agarose pads and add 3 µL of anesthetic (see step 3).
 3. Apply coverslip (worms are immobilized within 5 min).
 4. Seal the edges of the coverslip with melted adhesive sealant mixture (see **Table of Materials**).

5. Acquire images

1. Super-resolution acquisition

1. Use a laser-scanning confocal microscope equipped for super-resolution microscopy with a 63x/1.40 Plan-Apochromat oil objective lens to achieve a small pixel size (e.g., < 50 nm). Acquire Z-stacks using the step size recommended by the manufacturer's software (see **Table of Materials**).
2. Collect a series of optical sections that span the total volume of the DD ventral process (e.g., 15-20 slices at 0.19 μm step size or 2- 3 μm thick). Submit Z-stacks for image processing using the manufacturer's software and analyze images with a score higher than 7 (**Figure 1B**, **Figure 2** and **Figure 3**).

2. Nyquist acquisition

1. Use a laser scanning confocal microscope to select the optimal pixel size for the wavelength of light and numerical aperture of the objective lens in use (e. g., 40x/1.4 Plan Fluor oil objective).
NOTE: The smaller pixel size will reveal the fine structure of DD spines.
2. Submit stack for 3D deconvolution using Automatic algorithm (see **Table of Materials**) (**Figure 3**).

3. Use the smallest Z-step possible (e.g., determined by Piezo stage) because

oversampling in Z can yield sharper images after 3D deconvolution¹³.

5. Image analysis

1. Use appropriate image processing software (see **Table of Materials**) to create maximum intensity projections of the Z-stacks¹⁴.
2. Manually count the protrusions on the DD dendrite.
NOTE: Protrusions are perpendicular extensions from the main shaft (**Figure 1B**, arrowheads).
3. Determine the length of the DD dendrite scored to calculate the density of spines per 10 μm of DD dendrite (**Figure 1C**).
4. Classify spines as thin/mushroom, filopodial, stubby or branched (**Figure 2A**).
NOTE: Thin/mushroom spines exhibit a narrow base (neck) and a broader tip (head). Filopodial spines do not display a constricted base (no neck) but have a constant width. Stubby spines have a wide base and tip. Branched spines are protrusions with more than one tip.

2. Assessing activation of DD dendritic spines by presynaptic cholinergic signaling

1. Create transgenic worms using conventional techniques (e.g., microinjection)^{8,9}
 1. Use the *flp-13* promoter to drive expression of the Ca^{++} sensor, GCaMP6s, in DD neurons and the *unc-4* promoter to drive expression of Chrimson, a red-shifted channelrhodopsin, in presynaptic VA neurons (**Figure 4A**). See the list of plasmids in **Supplementary File 1**.
2. Prepare All-trans Retinal (ATR) and control plates.

NOTE: ATR is a required cofactor for Chrimson to function as an optogenetically activated ion channel.

1. Prepare 100 mM ATR stock solution in ethanol (100%). Store at -20 °C in 1 mL aliquots.
2. Under a laminar flow hood, add 300 µL of overnight OP50 bacterial culture and 0.25 µL of ATR to each 60 mm NGM (Nematode Growth Medium) nutrient agar plate and spread with a sterile glass rod.
3. For controls, add 300 µL of OP50 bacteria and 0.25 µL of ethanol (100%) to a separate group of NGM plates.
4. Let plates sit in hood at room temperature for 24 h (protected from ambient light) to allow bacterial growth.

NOTE: Plates can be used after the initial 24 h incubation or maintained at 4 °C to use within 5 days.

3. Setting-up the experiment

1. Place five NC3569 L4-stage larvae on OP50-seeded ATR or control plates that lack ATR and grow in darkness at 23°C.
2. Three days later, use a stereo dissecting microscope to confirm vulva development to pick L4 stage progeny from ATR and control plates for imaging as described in steps 2.4.1-2.4.3.
3. On a microscope slide, place 2 µL of 0.05 µm polybeads (2.5% solids w/v) (see **Table of Materials**).
4. Use a platinum wire ("worm pick") to add a small globule of super glue to the solution and swirl gently to generate filamentous "strands" of glue. Then add 3 µL of M9 buffer (**Figure 4B**).

5. Place approximately ten L4 larvae in the solution and apply a coverslip.

NOTE: Glue fibers will randomly contact worms and immobilize them after the coverslip is applied. Worms that are embedded in large globules of glue appear desiccated and should not be imaged.

6. Seal edges of coverslip as mentioned in step 1.4.4.

4. Recording of evoked Ca⁺⁺ transients in dendritic spines.

1. Use a spinning disk confocal microscope equipped with a sensitive CCD camera, a 100x TIRF oil objective lens, and 488 nm and 561 nm laser lines (see **Table of Materials**).
2. Adjust microscope stage to position DD spines in the focal plane.
3. Set-up time-lapse acquisition to illuminate the sample with 488 nm laser line every frame (for detecting GCaMP6s fluorescence) and the 561 nm laser line at periodic intervals (for Chrimson excitation).

NOTE: For example, use 488 nm light to capture consecutive snapshots (200 ms) of GCaMP6s signal coupled with a 200 ms pulse of 561 nm light every 5th frame (**Figure 4C-E**). With this configuration, GCaMP levels before and after each 561 nm pulse are detected ~1 s apart (200 ms of 488 nm laser to detect GCaMP before VA activation, 200 ms of 561 nm pulse to activate VA and ~600 ms to switch between laser lines and emission filters. With this set-up, VA neurons are activated every 2.5 s.

5. Analysis of *in vivo* Ca⁺⁺ imaging

1. Use 2D-deconvolution and image alignment to correct minor deviations arising from the worm

- movement during acquisition (see **Table of Materials**).
2. Define the DD dendritic spine as the Region Of Interest (ROI in **Figures 4C-D**).
 3. Duplicate the ROI and relocate to a neighboring region inside the worm to collect background signal (i.e., noise).
 4. Use appropriate software (see **Table of Materials**) to export GCaMP6s intensities to excel for each time point. Subtract background fluorescence from spine ROI fluorescence.
 5. Determine the change in fluorescence by subtracting the GCaMP6s fluorescence in the frame immediately before 561 nm excitation (F0) from each time-point after excitation (ΔF), then dividing by F0 to determine $\Delta F/F0$ (**Figure 4E**).
 6. Graph the normalized traces (See **Table of Materials**).
 7. Perform a paired statistical test for each measurement of GCaMP6s fluorescence before and after each pulse of 561 nm light.

- NOTE:** This approach effectively excludes random fluctuations in GCaMP6s fluorescence that otherwise reduce the statistical power of comparing the mean GCaMP6s signal from all measurements before and after 561 nm excitation (**Figure 4F**).
8. For measurements that show a normal or Gaussian distribution, use a paired parametric ANOVA test and correct for multiple comparisons for each of the two groups (ATR before vs. after, no ATR before vs. after). Alternatively, for data that are not normally distributed, use a non-parametric ANOVA with posthoc correction for multiple testing.

NOTE: Worms grown on plates that lack ATR ("no ATR") are necessary controls and should not show 561 nm-activated Ca^{++} transients because ATR is required for Chrimson function.

Representative Results

Measurements with three independent markers (cytosolic mCherry, LifeAct::GFP, MYR::mRuby) yielded an average density of 3.4 ± 1.03 DD dendritic spines per 10 μm of DD dendrite in wild-type young adults (**Figure 1B,C**). For this analysis, the measurements obtained with the GFP::Utrophin marker that yielded a significantly lower spine density were excluded (2.4 ± 0.74 , **Figure 1**) due to interactions of Utrophin with the actin cytoskeleton⁶ that potentially drives spine morphogenesis¹⁵. The measurements of spine density in the light microscope are comparable to the value of 4.2 spines/10 μm dendrite obtained from the reconstruction of 12 spines from electron micrographs of the DD1 neuron². The live-cell imaging approach confirmed that the thin/mushroom-shaped morphology of the DD spines predominates in the adult vs. alternative spine shapes (e.g., filopodial, stubby, branched) (**Figure 2B**), which is also typical for spines in the mature mammalian nervous system¹⁶.

An optogenetic strategy was used to ask if the presumptive dendritic spines detected by high-resolution light microscopy (**Figure 1** and **Figure 2**) are responsive to neurotransmitter release from presynaptic sites, a characteristic hallmark of dendritic spines in mammalian neurons. Green light (561 nm) was used to activate a channelrhodopsin variant, Chrimson, in presynaptic cholinergic neurons and blue light (488 nm) to detect Ca^{++} -dependent fluorescence emitted by a cytoplasmic GCaMP probe in postsynaptic DD dendritic spines. This experiment detected transient bursts of GCaMP signal in DD spines immediately after

optogenetic activation of Chrimson in presynaptic VA neurons (**Figure 3**). The success of this experiment depends on the reliable expression of Chrimson in all presynaptic VA neurons. In this case, a chromosomal integrant¹⁷ of the *Punc-4::Chrimson* marker was used to ensure consistent VA expression. This experiment could also be conducted with an extrachromosomal array. Chrimson expression in a specific VA neuron can be independently confirmed, for example, by coupling the Chrimson transgene to an SL2

transplanted leader sequence with a downstream nuclear-localized GFP as a co-expression marker². It is essential to perform a control experiment in the absence of ATR to confirm that the measured GCaMP signal depends on optogenetic activation of Chrimson, which is strictly ATR-dependent (**Figure 4D**). Finally, because evoked Ca⁺⁺ signals are transient, it is crucial to adopt an imaging protocol that allows rapid switching (<1 s) between 561 nm excitation and GCaMP signal acquisition with the 488 nm laser (**Figure 4**).

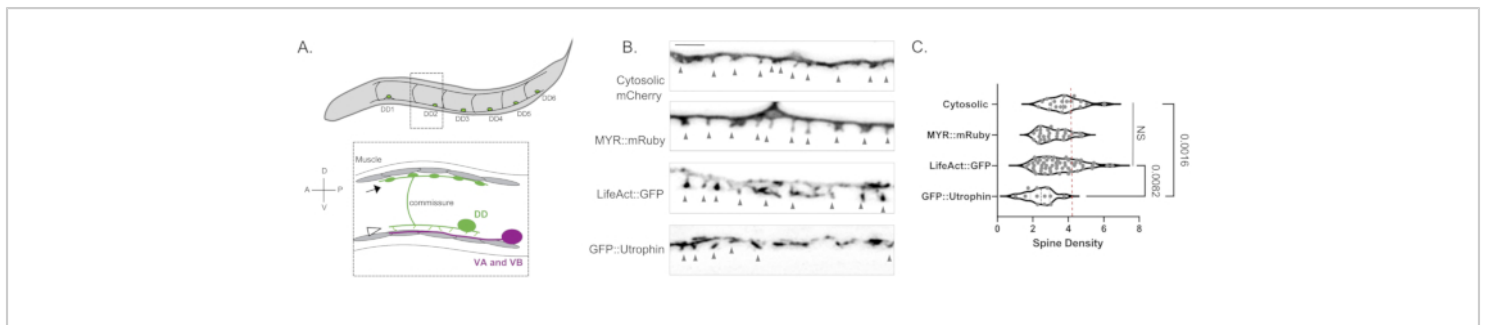


Figure 1: Labeling of DD dendritic spines. (A) (Top) Six Dorsal D (DD1-DD6) neurons in the ventral nerve cord of *C. elegans*. (Bottom) In adults, ventrally directed DD spines (arrowhead) contact presynaptic terminals of Ventral A (VA) and Ventral B (VB) motor neurons (magenta), and DD commissures extend to the dorsal nerve cord to provide GABAergic output to body muscles (arrow)¹⁸. This figure has been modified from Reference². (B) Fluorescent micrographs (Airyscan) of DD spines labeled with cytosolic mCherry, myristoylated mRuby (MYR::mRuby), LifeAct::GFP and GFP::Utrophin in young adult worms. Gray arrowheads point to spines. Scale bar = 2 μm. (C) Density (spines/10 μm) of DD neuron dendritic spines labeled with cytosolic mCherry (3.77 ± 0.9), MYR::mRuby (3.09 ± 0.8), LifeAct::GFP (3.44 ± 1.1) or GFP::Utrophin (2.41 ± 0.8). All samples are normally distributed. One-Way ANOVA shows that spine densities for cytosolic mCherry, MYR::mRuby, and LifeAct::GFP are not significantly (NS) different, whereas spine density is reduced for GFP::Utrophin vs. cytosolically labeled mCherry ($p = 0.0016$) and LifeAct::GFP ($p = 0.0082$). The dashed red line represents the spine density of DD neurons assessed from 3D EM reconstruction (4.2 spines/10 μm). This figure has been modified from Reference². [Please click here to view a larger version of this figure.](#)

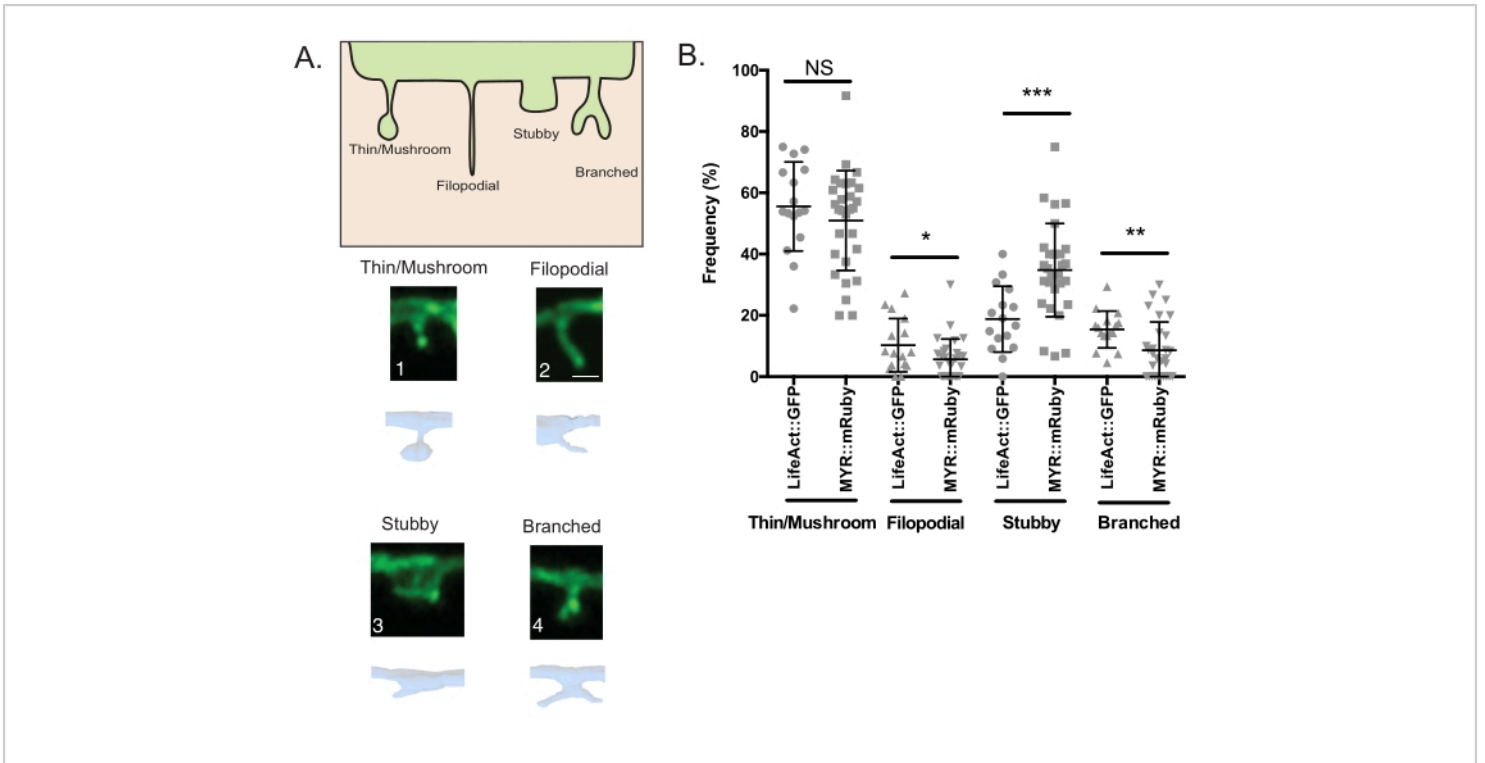


Figure 2: Imaging DD dendritic spines. (A) (Top) Schematic of spine shapes. (Bottom) Airyscan images of each type of spine (Scale bar = 500 nm) labeled with LifeAct::GFP (green) and 3D-reconstructions by serial electron micrographs of a high-pressure frozen adult (blue). (B) Spine frequency by type, visualized with LifeAct::GFP: Thin/Mushroom (55.5 ± 14.5%), Filopodial (10.3 ± 8.70%), Stubby (18.8 ± 10.7%), Branched (15.42 ± 6.01%). Spines frequency by type visualized with MYR::mRuby: Thin/Mushroom (52.2 ± 16.5%), Filopodial (5.68 ± 7.0%), Stubby (33.1 ± 14.8%), Branched (9.02 ± 9.6%). Unpaired T-test, Filopodial (p = 0.0339); Stubby (p = 0.0009) and Branched (p = 0.011) spines labeled with the MYR::mRuby marker are significantly different from LifeAct::GFP. This figure has been modified from Reference². Please click here to view a larger version of this figure.

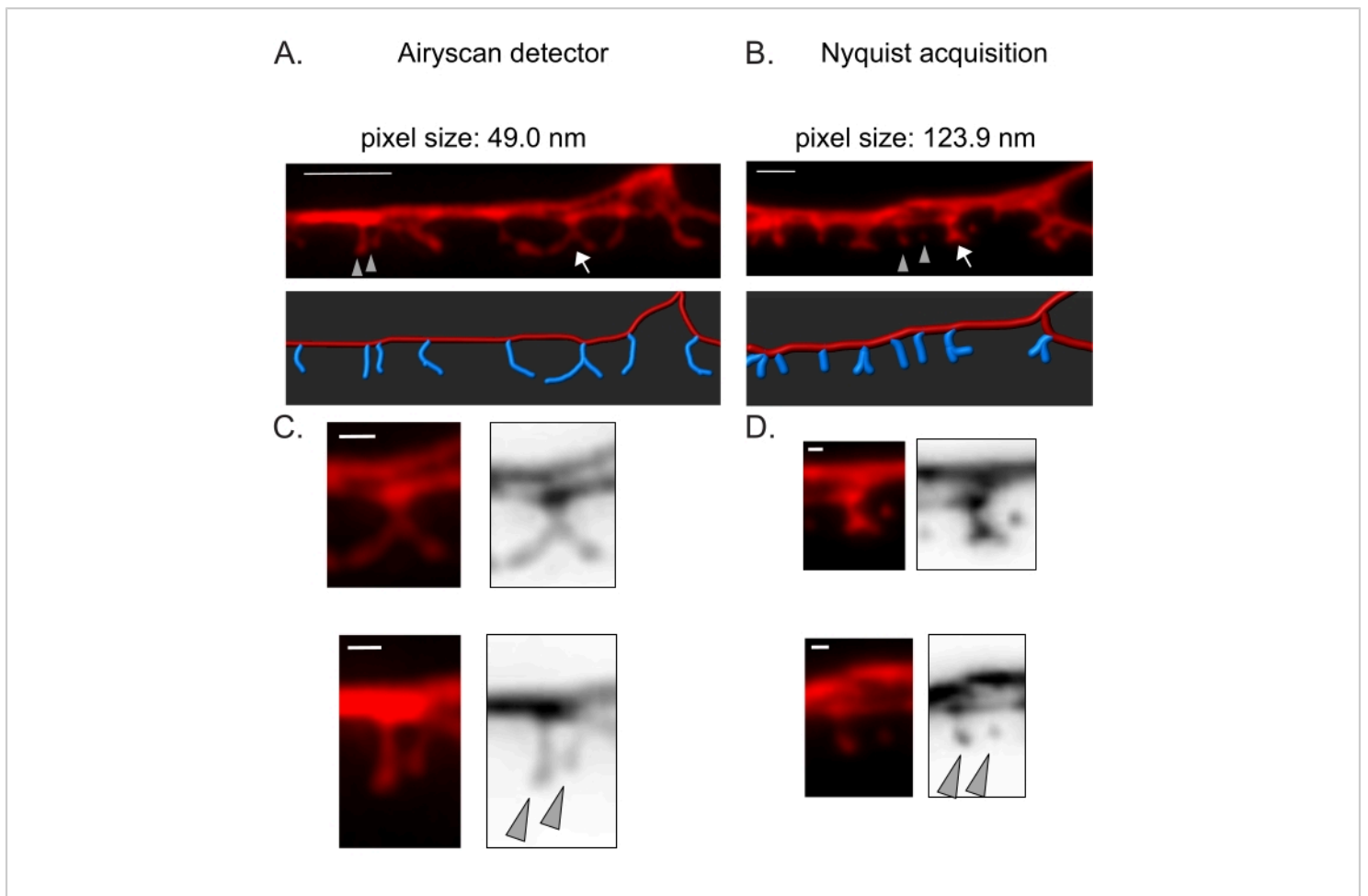


Figure 3: Strategies for acquiring high-resolution images of DD spines. (A-B) (Top) Fluorescent images of DD1 dendrites labeled with a cytosolic marker (mCherry) by (A) Airyscan detector and (B) Nyquist acquisition. (Bottom) DD dendrite (red) is depicted with an image analysis software (auto-path option of filament tracer), and DD spines (blue) are graphically illustrated using the semi-automated spines detection module. Arrow points to branched spine enlarged in C and D. Arrowheads denote neighboring thin/mushroom spines enlarged in C and D. Scale bar = 2 μm . (C-D) Enlarged examples of (top) branched spine (arrow) and (bottom) two neighboring thin/mushroom spines (arrowheads) obtained with (C) Airyscan detector or by (D) Nyquist acquisition. Scale bar = 500 nm. Data reproduced from². [Please click here to view a larger version of this figure.](#)

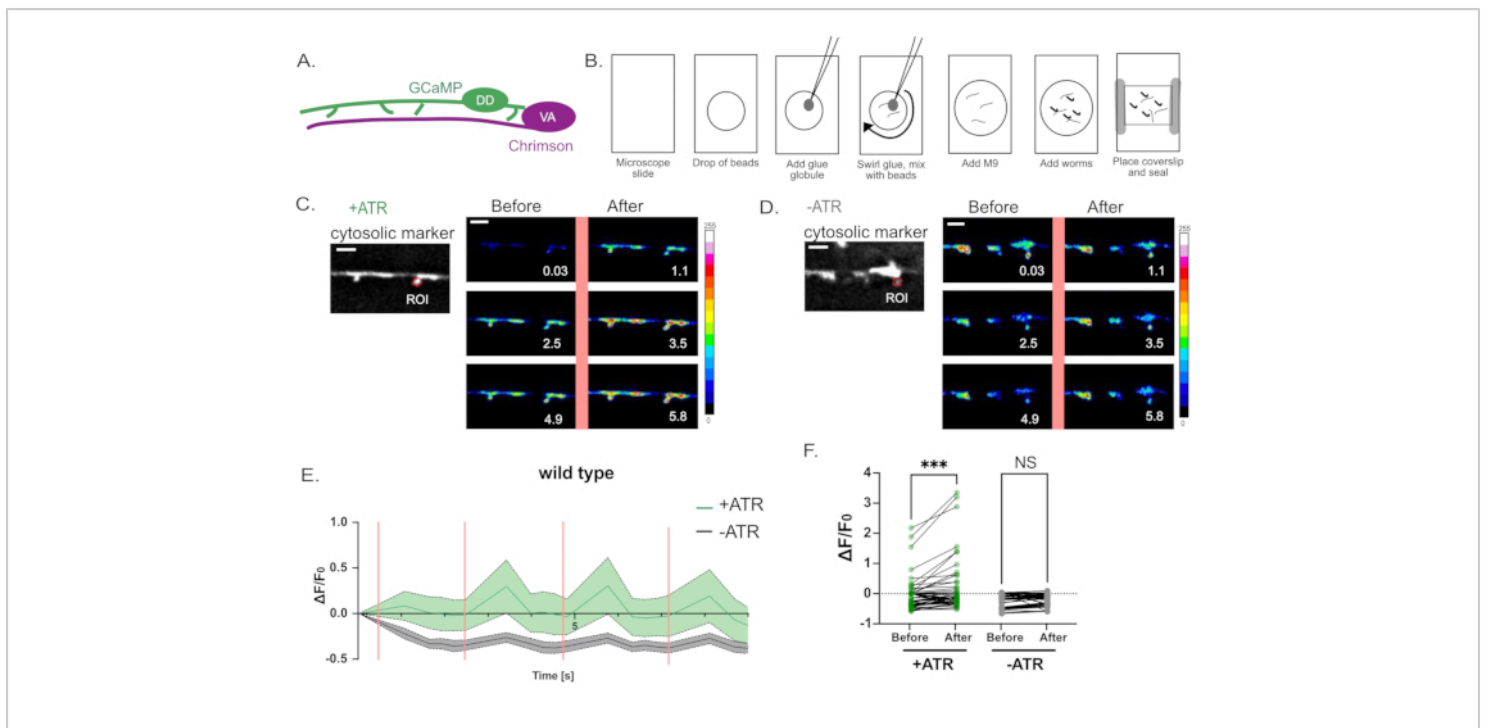


Figure 4: Assessing the function of DD spines. (A) DD motor neurons express the Ca^{++} indicator GCaMP6s (green), and VA motor neurons express the channelrhodopsin-variant, Chrimson (magenta)⁷. (B) Schematic depicting method for mounting worms for Ca^{++} measurements. (1) On a clean microscope slide, (2) place 2 μL of 0.05 μm poly beads, (3) use a platinum wire ("worm pick") to add a small globule of super glue and (4) swirl into the solution to generate filamentous strands of glue. (5) Add 3 μL of M9 buffer. (6) Place approximately ten L4 larvae in the solution, (7) apply coverslip and seal edges with Vaseline/wax. (C-D) Activation of VA neurons correlates with Ca^{++} transients in DD1 spines. GCaMP6s fluorescence imaged (at 0.5 s intervals) with periodic light activation of Chrimson (2.5 s intervals) evokes Ca^{++} transients with (C) +ATR (n = 12) but not in (D) controls (-ATR, n = 12). Panels are snapshots over time (s), before and after pulse of 561 nm light (vertical pink line). Scale bars = 2 μm . GCaMP6s signal is acquired from an ROI (Region of Interest) at the tip of each spine. (E) GCaMP6s fluorescence during the 10 s recording period plotted for +ATR (green) vs -ATR (control, gray) (n = 12 videos). Vertical pink bars denote 561 nm illumination (e.g., Chrimson activation). Each animal was stimulated 4 times with 561 nm light. Measurements were collected before and after each pulse of 561 nm light. (F) Plot of the GCaMP6s fluorescence before and after each pulse of 561 nm light. GCaMP6s fluorescence was measured 1 s after each pulse of 561 nm light. Because samples are not normally distributed, a paired non-parametric Friedman test was applied to correct for multiple comparisons of GCaMP6s fluorescence before vs. after 561 nm light stimulation for worms grown either with ATR (+ATR, green) (***) p = 0.0004, n = 48 measurements) or in the absence of ATR (-ATR, gray) (NS, Not Significant, p = 0.0962, n = 48 measurements). This figure has been modified from Reference². [Please click here to view a larger version of this figure.](#)

Supplementary File 1: List of plasmids used in the study.

[Please click here to download this File.](#)

Supplementary File 2: Composition and preparation of M9 buffer. [Please click here to download this File.](#)

Discussion

The Airyscan detector was selected to acquire snapshots of DD spines because it affords a higher signal-to-noise ratio and better resolution than conventional confocal microscopes^{19,20}. AiryScan imaging also allows the use of conventional fluorescent proteins (e.g., GFP, mCherry, etc.), now widely available for *C. elegans*. Although higher resolution images can be obtained with other super-resolution methods (e.g., STORM, STED, PALM), these methods require photo-activatable or photo-switchable fluorescent proteins²¹. As an alternative to Airyscan, conventional confocal microscopes are recommended. For example, imaging with Nyquist acquisition (**Figure 3**) achieves the pixel size using a 40x/1.3 objective of 123.9 nm, sufficient to distinguish the spine morphological types (**Figure 2**).

For determining spine density, using a cytosolic fluorescent protein such as (1) mCherry or GFP, (2) LifeAct to label the actin cytoskeleton, or (3) a myristoylated fluorescent protein (e.g., MYR::mRuby) to label the plasma membrane (**Figure 1B**) is recommended. In comparison, the F-actin binding protein Utrophin reduces spine density (**Figure 1C**), indicating a negative effect on spine morphogenesis when Utrophin is over-expressed.

The current imaging methods should help identify genetic variants that govern spine morphology^{1,16}. DD spine morphology (i.e., thin/mushroom, filopodial, stubby, branched, see **Figure 2**) can be assessed from single 2D-projections of the ventral nerve cord lateral images since

most DD spines adopt a characteristically ventrally-directed orientation. In these comparisons, it is essential to use the same fluorescent marker for each condition since apparent spine morphological types seem to be influenced by the labeling method (e.g., MYR::mRuby vs. LifeAct::GFP). In addition, it was noted that the spine shapes are dynamic and likely change shape in response to the external signals^{2,16}. Thus, it is also essential to compare spine shapes between genotypes at similar developmental stages and under similar conditions.

The orientation of the *C. elegans* ventral cord is critically vital for accurate image acquisition. Both the ventral and dorsal cords on opposite sides of the animal should be visible in the same Z-plane, indicating that the worm is oriented on its side (**Figure 1B**). It is best not to collect images of worms moving or in contact with other worms or bubbles near the ventral cord, as this can degrade images of spines.

For *in vivo* calcium imaging, fresh slides need to be prepared immediately before each acquisition. It is best to image worms in contact with only thin glue fibers vs. "globs" of glue which tend to desiccate worms and degrade the image (**Figure 4B**). In the experiment shown in **Figure 4**, the pulse of 561 nm light activates the entire field of view. For increasing the temporal and spatial resolution to detect local Ca⁺⁺ transients, for example, within individual DD spines, a galvo mini scanner set up for the 561 nm laser line can be used to stimulate a smaller region of interest¹⁷.

Disclosures

We declare no conflicts of interest.

Acknowledgments

Imaging and analysis on Imaris were performed in the Vanderbilt Cell Imaging Shared Resource (CIRS) supported by NIH (CA68485, DK20593, DK58404, DK59637, and EY08126). The LSM 880 is supported by grant 1S10OD201630. Imaging on a Nikon spinning disk was performed at the Nikon Center of Excellence. We thank Jenny Schafer, CIRS director, and Bryan Millis for training and insightful discussions and members of the Burnette lab: Dylan Burnette, Aidan Fenix, and Nilay Taneja for advice. This work was supported by National Institutes of Health grants to DMM (R01NS081259 and R01NS106951) and an American Heart Association grant to ACC (18PRE33960581).

References

1. Sala, C., Segal, M. Dendritic Spines: The Locus of Structural and Functional Plasticity. *Physiological Reviews*. **94** (1), 141-188 (2014).
2. Cuentas-Condori, A. et al. C. elegans neurons have functional dendritic spines. *Elife*. **8**, e47918 (2019).
3. Philbrook, A. et al. Neurexin directs partner-specific synaptic connectivity in C. Elegans. *Elife*. **7**, e35692 (2018).
4. Oliver, D., Alexander, K., Francis, M. M. Molecular Mechanisms Directing Spine Outgrowth and Synaptic Partner Selection in Caenorhabditis elegans. *Journal of Experimental Neuroscience*. **12**, 10-13 (2018).
5. Riedl, J. et al. Lifeact: a versatile marker to visualize F-actin. *Nature Methods*. **5**, 605-607 (2008).
6. Ladit, K., Ganguly, A., Roy, S. Axonal actin in action: Imaging actin dynamics in neurons. *Methods of Cell Biology*. **131**, 91-106 (2016).
7. Schild, L. C., Glauser, D. A. Dual color neural activation and behavior control with chrimson and CoChR in *Caenorhabditis elegans*. *Genetics*. **200** (4), 1029-1034 (2015).
8. Mello, C., Kramer, J., Stinchcomb, D., Ambros, V. Efficient gene transfer in C. elegans: extrachromosomal maintenance and integration of transforming sequences. *The EMBO Journal*. **10** (12), 3959-3970 (1991).
9. Berkowitz, L. A., Knight, A. L., Caldwell, G. A., Caldwell, K. A. Generation of Stable Transgenic C. elegans Using Microinjection. *Journal of Visualized Experiments*. **18**, e833 (2008).
10. Smith, C. J. et al. Time-lapse imaging and cell-specific expression profiling reveal dynamic branching and molecular determinants of a multi-dendritic nociceptor in C. elegans. *Developmental Biology*. **345** (1), 18-33 (2010).
11. Mccarter, J., Bartlett, B., Dang, T., Schedl, T. Soma - Germ Cell Interactions in Caenorhabditis elegans: Multiple Events of Hermaphrodite Germline Development Require the Somatic Sheath and Spermathecal Lineages. *Developmental Biology*. **181** (2), 121-143 (1997).
12. Driscoll, M. Mounting animals for observation with Nomarski DIC optics. *WormBook*. (2008).
13. North, A. J. sing is believing? A beginners' guide to practical pitfalls in image acquisition. *Journal of Cell Biology*. **172** (1), 9-18 (2006).
14. Schindelin, J. et al. Fiji: An open-source platform for biological-image analysis. *Nature Methods*. **9**, 676-682 (2012).
15. Hotulainen, P., & Hoogenraad, C. C. Actin in dendritic spines: connecting dynamics to function. *Journal of Cell Biology*. **189** (4), 619-629 (2010).

16. Berry, K. P., Nedivi, E. Spine Dynamics: Are They All the Same? *Neuron*. **96** (1), 43-55 (2017).
17. Miller, D. M., Niemeyer, C. J. Expression of the unc-4 homeoprotein in *Caenorhabditis elegans* motor neurons specifies presynaptic input. *Development*. **121** (9), 2877-2886 (1995).
18. White, J. G., Southgate, E., Thomson, J. N., Brenner, S. The Structure of the Ventral Nerve Cord of *Caenorhabditis elegans*. *Philosophical Transactions of the Royal Society*. **275** (938), 327-348 (1976).
19. Huff, J. The Airyscan detector from ZEISS: confocal imaging with improved signal-to-noise ratio and super-resolution. *Nature Methods*. **12**, i-ii (2015).
20. Huff, J. The Fast mode for ZEISS LSM 880 with Airyscan: high-speed confocal imaging with super-resolution and improved signal-to-noise ratio. *Nature Methods*. **13**, i-ii (2016).
21. Jacquemet, G., Carisey, A. F., Hamidi, H., Henriques, R., Leterrier, C. The cell biologist's guide to super-resolution microscopy. *Journal of Cell Science*. **133** (11) jcs240713 (2020).